

Towards Understanding Preservation of Periodic Object Motion in Computed Tomography

Franziska Schirmmacher^{1,*}, Oliver Taubmann^{1,2,*}, Mathias Unberath^{1,2}, and Andreas Maier^{1,2}

¹ Pattern Recognition Lab, Department of Computer Science,
Friedrich-Alexander-University Erlangen-Nuremberg, Germany

² Graduate School in Advanced Optical Technologies (SAOT), Erlangen, Germany

* These authors contributed equally to this work.

{franziska.schirmmacher,oliver.taubmann}@fau.de

Abstract. In this paper, we study periodic object motion in computed tomography. Specifically, we investigate the phenomenon that motion may—in a sense—be preserved even in a standard analytical reconstruction that assumes a static object. In fact, these preserved motion patterns *reappear* in a forward-projection of the allegedly static reconstruction. In numerical simulations abstracting the cardiac anatomy, we show that not only the type of motion, but also the sharpness of the boundary of the moving object affects how much of the motion is preserved.

1 Introduction

Computed tomography (CT) imaging of the heart typically entails a challenging image reconstruction problem. While the radiation source rotates around a patient, their heart beats. This leads to inconsistencies in the acquired data and results in artifacts when performing a straight-forward reconstruction [1–3]. Different types of motion may be observed in a cardiac scan; the ventricles contract periodically, whereas the coronary arteries or catheters inserted into the heart mostly exhibit translational motion caused by the contraction [4]. Naturally, the sizes and shapes of the moving objects vary considerably as well. Arteries and catheters are narrow, elongated structures with a relatively sharp response characteristic, i. e. the image gradient at the object edges is high, and they are often displaced by a distance at least as large as their own diameter, while their shape remains mostly unaffected. In contrast, the ventricles usually do not have boundaries that are as well-defined and they describe a pulsating motion pattern, causing the object to change its size and shape.

In a standard reconstruction that assumes a static object, these differences lead to the ventricles appearing blurred, while arteries or catheters tend to cause streaking artifacts [3]. Curiously, in a forward projection of such an image using the same trajectory, the ventricles appear largely stationary while the catheter follows its original motion to a certain extent. An illustrative example is shown in Fig. 1. In this paper, we aim to identify properties relevant to this phenomenon and quantify their influence using numerical simulations.

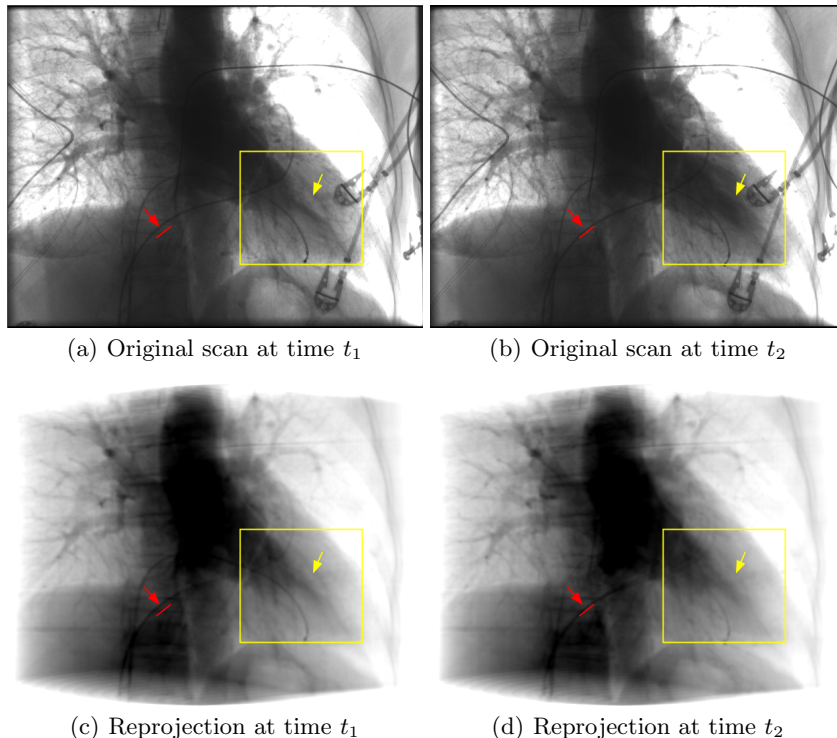


Fig. 1. Frames of a rotational angiogram (a, b) and corresponding digitally reconstructed radiographs (DRR) obtained via projection of a *static* reconstruction (c, d). Note that the catheter still follows its original motion (red) in the DRR, whereas the left ventricle no longer pulsates (yellow). The full scan covers ca. 27 heart beats.

2 Materials and Methods

2.1 A Simple Dynamic Phantom

The phantom used in our simulations consists in a temporally varying circle. Blurring the edges of the circle by convolution with a Gaussian filter kernel yields different versions with varying sharpness. Modifiable parameters for each circle are its center $\boldsymbol{\mu} = (\mu_x, \mu_y)^\top$, its radius r , the number of motion periods f during the acquisition, and the standard deviation of the Gaussian σ .

These parameters allow for a dynamic simulation adapted to the properties of cardiac motion. We define motion by two extremal states between which a parameter oscillates following a sinusoidal curve. As a consequence, $r(t)$, $\boldsymbol{\mu}(t) \propto \cos(2\pi \cdot f \cdot t)$ are time dependent, with $t \in [0, 1]$ being the time relative to the complete acquisition.

Two different dynamic objects, \mathbf{O}_{puls} and $\mathbf{O}_{\text{shift}}$, are considered, which roughly mimic the behavior of ventricles and arteries/catheters, respectively. \mathbf{O}_{puls} is centered at the origin, $\boldsymbol{\mu} = (0, 0)^\top$, and pulsates with its radius ranging from

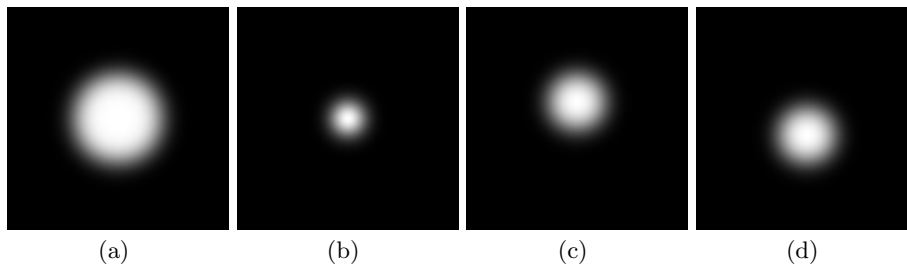


Fig. 2. Extremal states of the motion patterns of both considered objects $\widehat{\mathbf{O}}_{\text{puls}}$ (a, b) and $\widehat{\mathbf{O}}_{\text{shift}}$ (c, d), with $\sigma = 5$.

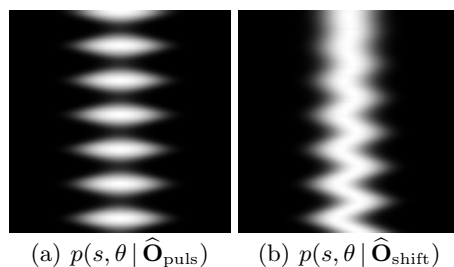


Fig. 3. Sinograms for $f = 23$ and $\sigma = 5$. The angular range $\theta \in [0^\circ, 50^\circ]$ is shown.

r_{\min} to r_{\max} . $\mathbf{O}_{\text{shift}}$ retains its shape with a fixed radius $r_c = (r_{\max} + r_{\min})/2$ corresponding to the mean radius of \mathbf{O}_{puls} over time. Its position ranges from $(0, -\mu_s)^\top$ to $(0, \mu_s)^\top$, where $\mu_s = r_{\max} - r_c$ to ensure that the maximum extents of both objects w.r.t. the origin coincide. Fig. 2 displays the extremal motion states of both objects after blurring with the 2-D Gaussian kernel \mathbf{G}_σ ,

$$\widehat{\mathbf{O}}_\diamond = \mathbf{O}_\diamond * \mathbf{G}_\sigma, \quad \diamond \in \{\text{puls}, \text{shift}\}. \quad (1)$$

We then compute the Radon transform to obtain a parallel-beam sinogram $p(s, \theta)$ over $\theta \in [0^\circ, 180^\circ]$,

$$p(s, \theta | \widehat{\mathbf{O}}_\diamond) = \iint \widehat{\mathbf{O}}_\diamond(\boldsymbol{\mu}(t_\theta), r(t_\theta)) \cdot \delta(y \cos(\theta) + x \sin(\theta) - s) dx dy, \quad (2)$$

where δ denotes the Dirac delta function and $t_\theta = \theta/180^\circ$. Example sinograms are shown in Fig. 3.

2.2 Reconstruction and Reprojection

Filtered back-projection using the standard Ram-Lak convolver [5] is employed to obtain a (motion-corrupted) reconstruction \mathbf{R}_\diamond from each sinogram. Subsequently, we project the reconstructed image forward again with the same acquisition geometry. Although generated from a static image, it can be observed

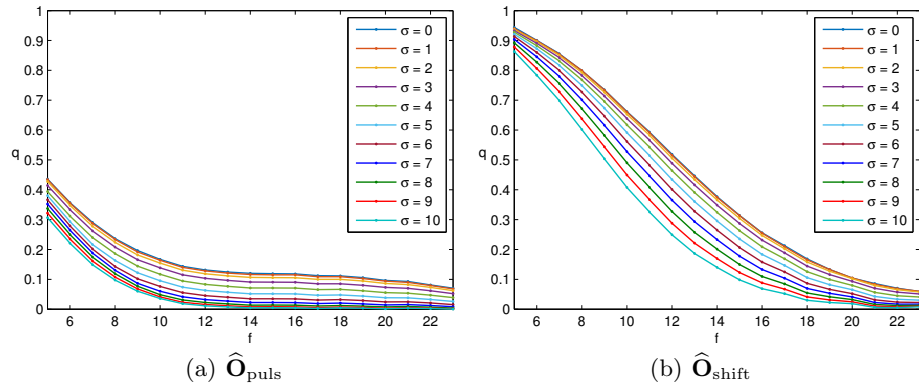


Fig. 4. Plots of the fraction of preserved motion q over the frequency f for different values of σ , which controls the edge sharpness.

that this reprojected sinogram may retain a fraction of the original motion. It is, therefore, compared to the original sinogram in terms of the amount of periodic motion it still contains.

To obtain a quantitative measure for this property, we consider the point $(0, r_c)^\top$, located on the boundary of both objects in their mean state of motion, and collect all line integrals through this point observed in both the original and reprojected sinograms as two sequences \mathbf{s}_{orig} , $\mathbf{s}_{\text{reproj}}$, respectively. On both sequences, the 1-D Fourier transform \mathcal{F} is performed to obtain the energy associated with the frequency f of the simulated motion. To increase the robustness of the measure, nearby frequencies are considered as well. More precisely, the Fourier-transformed sequences are multiplied element-wise with a 1-D Gaussian function with mean f and standard deviation of unity and, finally, summed up as $\xi_f(\mathcal{F}\{\mathbf{s}_{\text{orig}}\})$ and $\xi_f(\mathcal{F}\{\mathbf{s}_{\text{reproj}}\})$. To quantify the remaining motion in the reprojected sinogram, we compute their ratio

$$q = \frac{\xi_f(\mathcal{F}\{\mathbf{s}_{\text{reproj}}\})}{\xi_f(\mathcal{F}\{\mathbf{s}_{\text{orig}}\})}. \quad (3)$$

2.3 Parameter Values

We set $r_{\min} = 5$ and $r_{\max} = 20$, resulting in $r_c = 12.5$ and $\mu_s = 7.5$. For σ and f all integers in the ranges $[0, 10]$ and $[5, 23]$ are considered, respectively. Frequencies $f \leq 4$, for which a period would cover at least 45° of the trajectory, were not evaluated to keep the focus on cases where the motion is markedly faster than rotational effects. For all possible combinations of both of these parameters, q is calculated to comprehensively assess their influence on the amount of motion preserved. The phantom images are 300×300 pixels large. The acquisition was simulated with an angular spacing of 0.5° and 500 detector elements.

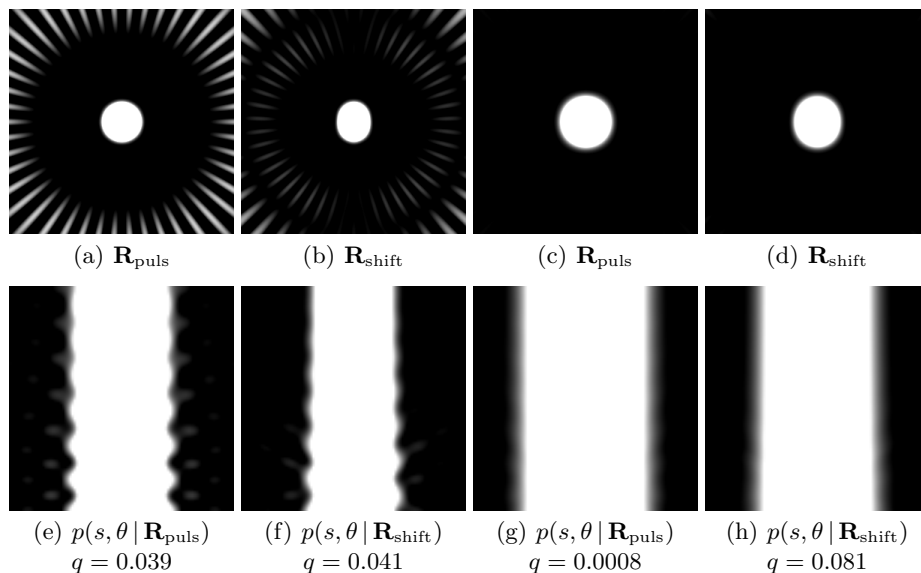


Fig. 5. Reconstructed images (top row) and reprojected sinograms (bottom row) displayed with a bright, high-contrast windowing to emphasize artifacts, where $\sigma = 5$ for (a, b, e, f) and $\sigma = 10$ for (c, d, g, h). In all images, $f = 23$ cycles were simulated. The sinograms are shown in the angular range $\theta \in [0^\circ, 50^\circ]$.

3 Results

The quantitative results of the simulation are summarized in Fig. 4. For both motion types, higher fractions q of the original motion are retained for lower frequencies f . The predominant trend is that this effect is much stronger for the translational than for the pulsating movement, which is intuitively in line with what can be observed from catheters and ventricles in real data (cf. Fig. 1).

However, it is important to note that at higher frequencies, the influence of edge sharpness gradually increases and finally surpasses that of the motion type. E. g., for $f = 23$, a sharper $\hat{\mathbf{O}}_{\text{puls}}$ at $\sigma = 5$ exhibits substantially more motion after reconstruction and reprojection than a smoother $\hat{\mathbf{O}}_{\text{shift}}$ at $\sigma = 10$, both in terms of the quantitative measurement and visual impression (see Fig. 5). In fact, the difference in edge sharpness is more likely to explain what is observed in Fig. 1 as the real scan covers 27 cycles, falling into a similar frequency regime.

In addition, looking at the reconstructed images Fig. 5(a) and Fig. 5(b), it seems reasonable to assume that the preservation of motion in the static image is closely linked to the streaking artifacts typically observed in motion-corrupted scans. In other words, the streaks “encode” the original motion, which could be a valuable insight when designing methods to deal with this effect. A practical consequence of this issue, seen in Fig. 5(e), is the angle-dependence of the preserved motion due to the rotational asymmetry of Fig. 5(a). It also implies that the grid size contributes to the occurrence of this effect.

4 Discussion

In summary, this work is concerned with the phenomenon that periodic motion of a dynamic object may be preserved even within a static reconstruction. We were able to reproduce observations made in complex real-world data sets within a simple simulation framework, where we quantified the contribution of two properties of the dynamic object on this effect: The type of motion (translational vs. pulsating) and the sharpness of its boundaries. While both were influential, we found that the relative strength of their influence is highly dependent on the motion frequency.

Our findings can help foster a better understanding of the applicability and limitations of techniques which directly rely on a static reconstruction of dynamic objects as an intermediate step. Prominent examples are the artifact reduction method by McKinnon and Bates [6], prior image constrained compressed sensing [7], or joint bilateral filtering using a static guidance image [8]. Considering the importance of edge sharpness discovered in our simulations, investigating specialized reconstruction filters may be worthwhile, the design of which could be informed by artifact models in the spirit of, e.g., prior work on perfusion imaging [9].

References

1. Hansis E, Schäfer D, Dössel O, Grass M. Projection-based motion compensation for gated coronary artery reconstruction from rotational x-ray angiograms. *Physics in Medicine and Biology*. 2008;53(14):3807–3820.
2. Schwemmer C, Rohkohl C, Lauritsch G, Müller K, Hornegger J. Residual motion compensation in ECG-gated interventional cardiac vasculature reconstruction. *Physics in Medicine and Biology*. 2013;58(11):3717–3737.
3. Müller K, Maier A, Schwemmer C, Lauritsch G, Buck SD, Wielandts JY, et al. Image artefact propagation in motion estimation and reconstruction in interventional cardiac C-arm CT. *Physics in Medicine and Biology*. 2014;59(12):3121–3138.
4. Unberath M, Aichert A, Achenbach S, Maier A. Virtual Single-frame Subtraction Imaging. In: *Proc. Intl. Conf. on Image Formation in X-ray CT*; 2016. p. 89–92.
5. Zeng GL. *Medical Image Reconstruction : A Conceptual Tutorial*. Springer; 2010.
6. Mc Kinnon GC, Bates RHT. Towards Imaging the Beating Heart Usefully with a Conventional CT Scanner. *IEEE Transactions on Biomedical Engineering*. 1981;BME-28(2):123–127.
7. Chen GH, Tang J, Leng S. Prior image constrained compressed sensing (PICCS): a method to accurately reconstruct dynamic CT images from highly undersampled projection data sets. *Medical Physics*. 2008;35(2):660–663.
8. Taubmann O, Maier A, Hornegger J, Lauritsch G, Fahrig R. Coping with Real World Data: Artifact Reduction and Denoising for Motion-Compensated Cardiac C-arm CT. *Medical Physics*. 2016;43(2):883–893.
9. Fieselmann A, Dennerlein F, Deuerling-Zheng Y, Boese J, Fahrig R, Hornegger J. A model for filtered backprojection reconstruction artifacts due to time-varying attenuation values in perfusion C-arm CT. *Physics in Medicine and Biology*. 2011;56(12):3701–3717.